# Energy and rotation-dependent stereodynamics of $H(^2S) + NH(a^1\Delta) \rightarrow H_2(X^1\Sigma_g^+) + N(^2D)$ reaction*

Yong-Qing Li(李永庆)[1,2,†], Yun-Fan Yang(杨云帆)[1], Yang Yu(于洋)[1], Yong-Jia Zhang(张永嘉)[1], and Feng-Cai Ma(马凤才)[1,‡]

[1] *Department of Physics, Liaoning University, Shenyang* 110036, *China*

[2] *State Key Laboratory of Molecular Reaction Dynamics, Dalian Institute of Chemical Physics, Chinese Academy of Sciences, Dalian* 116023, *China*

(Received 26 July 2015; revised manuscript received 26 October 2015; published online 10 January 2016)

Quasi-classical trajectory calculations are performed to study the stereodynamics of the $H(^2S)$ + NH $(a^1\Delta) \rightarrow H_2(X^1\Sigma_g^+)$ + N $(^2D)$ reaction based on the first excited state $NH_2(1^2A')$ potential energy surface reported by Li *et al.* [Li Y Q and Varandas A J C 2010 *J. Phys. Chem. A* **114** 9644] for the first time. We observe the changes of differential cross-sections at different collision energies and different initial reagent rotational excitations. The influence of collision energy on the $\boldsymbol{k}$–$\boldsymbol{k}'$ distribution can be attributed to a purely impulsive effect. Initial reagent rotational excitation transforms the reaction mechanism from insertion to abstraction. The effect of initial reagent rotational excitations on $\boldsymbol{k}$–$\boldsymbol{k}'$ distribution can be explained by the rotational excitation enlarging the rotational rate of reagent NH in the entrance channel to reduce the probability of collision between incidence H atom and H atom of target molecular. We also investigate the changes of vector correlations and find that the rotational angular momentum vector $\boldsymbol{j}'$ of the product $H_2$ is not only aligned, but also oriented along the $y$ axis. The alignment parameter, the disposal of total angular momentum and the reaction mechanism are all analyzed carefully to explain the polarization behavior of the product rotational angular moment.

**Keywords:** differential cross section, stereodynamics, rotational excitation, rotational polarization, Vector correlation

**PACS:** 34.50.Lf, 34.50.–s, 31.15.xv **DOI:** 10.1088/1674-1056/25/2/023401

## 1. Introduction

The reaction H + NH $\rightarrow$ $H_2$ + N has played an important role in the chemistry of nitrogen containing fuels, the catalyst realm and the renewable energy production.[1] Owing to their significant effects, the ground and first excited electronic state of $NH_2$ have been studied quite extensively by various experimental[2–5] and theoretical techniques.[6–33] In the previous theoretical studies, most of them mainly forced on the dynamic behaviors of the ground and first excited state $NH_2$. In this case, such studies have often been concentrated on the scalar properties of the H + NH $\rightarrow$ $H_2$ + N reaction. To comprehensively understand the $NH_2$dynamics, it is insufficient to investigate only the scalar properties. Vector correlation can provide the detailed information about the whole atom motion when reaction occurs, which can help experimentalists rationalize the experimental results. So it is important to study not only their scalar properties, but also their vector properties. The most familiar vector correlation between the reagent and product relative velocity $(\boldsymbol{k}, \boldsymbol{k}')$ is characterized by the differential cross-section $d\sigma/d\omega_t$ (DCS), and the most important vector correlation is the correlation among three vectors $\boldsymbol{k}$, $\boldsymbol{k}'$, and $\boldsymbol{j}'$ (the product rotational angular momentum). The correlations among the three vectors in the center-of-mass (CM) frame can be characterized by certain interesting double and triple vector correlations.

In order to fully comprehend the excited-state property of $NH_2$ reaction Li and Varandas[6] reported an adiabatic PES of $NH_2$ first excited state $1^2A'$ based on the double many-body expansion (DMBE) theory. In the present work, the quasi-classical trajectory (QCT) method is used to mainly explore the vector correlations (such as $P(\theta_r)$, $P(\phi_r)$, and $P(\theta_r, \phi_r)$) based on the first excited state $NH_2(1^2A')$ DMBE-SEC PES.[6] We select three different collision energies (10, 20, and 30 kcal/mol) to investigate the influences on stereodynamics with $v = 0$ and $j = 0$. In turn, four different initial rotational levels ($j = 0$, 3, 6, 9) are chosen to further study the different effects originating from rotational excitation under the collision energy 30 kcal/mol with initial vibrational level $v = 0$. The rest of this paper is organized as follows. In Section 2 we briefly review the theoretical methodologies adopted in the current study. In Section 3 we present and discuss the calculated results. Finally, in Section 4 we draw some conclu-

*Project supported by the National Natural Science Foundation of China (Grant Nos. 11474141and 11274149), the Program for Liaoning Excellent Talents in University, China (Grant No. LJQ2015040), the Scientific Research Foundation for the Returned Overseas Chinese Scholars, State Education Ministry, China (Grant No. 2014-1685), and the Special Fund Based Research New Technology of Methanol Conversion and Coal Instead of Oil and the China Postdoctoral Science Foundation (Grant No. 2014M550158).

†Corresponding author. E-mail: yqli@lnu.edu.cn

‡Corresponding author. E-mail: fcma@lnu.edu.cn

© 2016 Chinese Physical Society and IOP Publishing Ltd 

sions from the present studies.

## 2. Theory

### 2.1. Quasi-classical trajectory calculations

The accurate first excited state $1^2A'$ PES constructed by Li and Varandas[6] is adopted in the present calculations. The calculation method of QCT is the same as that in Refs. [7]–[12]. In this work, three different collision energies (10, 20, and 30 kcal/mol) are selected to investigate the influences on stereodynamics with $v = 0$ and $j = 0$. In turn, four different initial rotational levels ($j = 0$, 3, 6, 9) are chosen to further study the different effects originating from rotational excitation under the collision energy 30 kcal/mol with $v = 0$. The classical Hamilton equations are numerically integrated in three dimensions. In our calculations, the integration step is set to be 0.1 fs to ensure a conservation of the results. In order to ensure no interaction between attacking atom H and the center-of-mass (CM) reference frame of the diatomic molecule NH, the distance between them is set to be 15 Å. A total of $3 \times 10^4$ trajectories are sampled, and the appropriate value of the maximum impact parameter is selected after preliminary running batches of $3 \times 10^3$ trajectories at each collision energy. The orientation of the diatomic molecule and the phase of the diatomic vibrational motion are randomly sampled by a Monte Carlo procedure. Moreover, the impact parameters are optimized before running the trajectories. That is to say, the initial azimuthal angle and polar angle of the reagent molecule internuclear axis are randomly sampled based on Monte Carlo method, and the range of the angles is from 0° to 180° and from 0° to 360°, respectively.

### 2.2. Vector correlations

The CM reference frame is used in the present investigation. The reagent initial relative velocity vector $\boldsymbol{k}$ is parallel to the $z$ axis in the CM frame. Scattering plane $x$–$z$ contains $\boldsymbol{k}$ and final product's relative velocity vector $\boldsymbol{k}'$. Scattering angle $\theta_t$ is the angle between $\boldsymbol{k}$ and $\boldsymbol{k}'$. The azimuthal and polar angles describing the direction of the final rotational angular moment $\boldsymbol{j}'$ are $\phi_r$ and $\theta_r$, respectively.

The distribution function of $P(\theta_r)$ describing the $\boldsymbol{k}$–$\boldsymbol{j}'$ correlation can be expanded in a series of Legendre polynomials as follows:[34–43]

$$P(\theta_r) = \frac{1}{2}\sum_k (2k+1) a_0^{(k)} \mathrm{P}_k(\cos\theta_r). \tag{1}$$

The coefficients of the expansion are given by

$$a_0^{(k)} = \int_0^{\pi} P(\theta_r)\mathrm{P}_k(\cos\theta_r)\sin\theta_r \mathrm{d}\theta_r = \langle \mathrm{P}_k(\cos\theta_r)\rangle, \tag{2}$$

when $k$ is odd, $a_0^{(k)}$ is called orientation parameter, and when $k$ is even, it is called alignment parameter. For $k = 2$, the coefficient of the expansion is

$$a_0^{(2)} = \langle \mathrm{P}_2(\cos\theta_r)\rangle = \langle P_2(\boldsymbol{j}\cdot\boldsymbol{k})\rangle = \frac{1}{2}\langle 3\cos^2\theta_r - 1\rangle, \tag{3}$$

which gives a simple way to express the degree of the product rotational alignment effect, and $a_0^{(2)}$ is called the rotational alignment parameter of the product.

The dihedral angle distribution function of $P(\phi_r)$ describing the $\boldsymbol{k}$–$\boldsymbol{k}'$–$\boldsymbol{j}'$ correlation can be expanded in a Fourier series[34–43]

$$P(\phi r) = \frac{1}{2\pi}\left(1 + \sum_{\text{even},n\geq 2} a_n \cos n\phi r + \sum_{\text{odd},n\geq 1} b_n \sin n\phi r\right), \tag{4}$$

where

$$a_n = 2\langle \cos n\phi_r\rangle \quad \text{and} \quad b_n = 2\langle \sin n\phi_r\rangle. \tag{5}$$

The joint probability density function of angles $\theta_r$ and $\phi_r$, which determine the direction of $\boldsymbol{j}'$, can be expressed as

$$\begin{aligned} P(\theta_r,\varphi_r) &= \frac{1}{4\pi}\sum_{kq}[k]a_q^k C_{kq}(\theta_r,\varphi_r)^* \\ &= \frac{1}{4\pi}\sum_k\sum_{q\geq 0}\left[a_{q\pm}^k \cos q\varphi_r - i a_{q\mp}^k \sin q\varphi_r\right] \\ &\quad \times C_{kq}(\theta_r,0), \end{aligned} \tag{6}$$

where $[k] = (2k+1)$, and the polarization parameter is expressed as

$$a_{q\pm}^k = 2\left\langle C_{k|q|}(\theta_r,0)\cos q\phi_r\right\rangle, \quad k \text{ is even}, \tag{7}$$

$$a_{q\mp}^k = 2\mathrm{i}\left\langle C_{k|q|}(\theta_r,0)\sin q\phi_r\right\rangle, \quad k \text{ is odd}. \tag{8}$$

The full three-dimensional angular distribution associated with $\boldsymbol{k}$–$\boldsymbol{k}'$–$j'$ can be represented by a set of generalized polarization dependent differential cross-sections (PDDCSs) in the CM frame that is described in Refs. [34]–[43]. The fully correlated CM angular distribution is written as

$$P(\omega_t,\omega_r) = \sum_{kq}\frac{[k]}{4\pi}\frac{1}{\sigma}\frac{\mathrm{d}\sigma_{kq}}{\mathrm{d}\omega_t}C_{kq}(\theta_r,\phi_r)^*, \tag{9}$$

where

$$\frac{1}{\sigma}\frac{\mathrm{d}\sigma_{00}}{\mathrm{d}\omega_t} = \frac{1}{4\pi}\sum_{k_1}[k_1]\left\langle \mathrm{P}_{k_1}(\cos\theta_t)\right\rangle \mathrm{P}_{k_1}(\cos\theta_t), \tag{10}$$

$$\frac{1}{\sigma}\frac{\mathrm{d}\sigma_{20}}{\mathrm{d}\omega_t} = \frac{1}{4\pi}\sum_{k_1}[k_1]\left\langle \mathrm{P}_{k_1}(\cos\theta_t)\right\rangle \mathrm{P}_{k_1}(\cos\theta_t). \tag{11}$$

## 3. Results and discussion

### 3.1. $\boldsymbol{k}$–$\boldsymbol{k}'$ vector correlations

Figure 1 shows the global $\boldsymbol{k}$–$\boldsymbol{k}'$ angular distribution for the DMBE-SEC PES. The calculated DCS values for the H($^2$S) + NH ($a^1\Delta$) → H$_2$($X^1\Sigma_g^+$) + N ($^2$D) reaction at three collision energies are displayed in Fig. 1(a). It is clearly shown

that the HH molecules are scattered mainly in the broad forward and backward. A similar forward-backward scattering has been reported by Peyerimhoff and Buenker in the $NH_2$ ground state PES.[15] With the increase of the collision energy, both forward scattering and backward scattering become higher, in which the forward scattering has a bigger magnitude of variation. According to the capture model,[44] it may be easy to understand that the forward scattering increases with the increase of collision energy. The influence of collision energy on the $\boldsymbol{k}$–$\boldsymbol{k}'$ distribution can be attributed to a purely impulsive effect. At higher energies, more repulsive regions of the surface become available. More repulsive parts of the PES energetically accessible are not compensated for by increasing the collision energies, resulting in a forward scattering tendency with the increase of collision energy. The variations of the $\boldsymbol{k}$–$\boldsymbol{k}'$ angular distribution with rotational level ($v = 0$, $j = 0$, 3, 6, 9) for NH molecular at collision energy of 30 kcal/mol are shown in the plot of Fig. 1(b). As can be seen in Fig. 1(b), both forward and backward scattering become lower with the increase of rotational quantum number. It could be explained as the fact that the rotational excitation enlarges the rotational rate of reagent NH in the entrance channel, which reduces the probability of collision between incident H atom and H atom of target molecular, resulting in both forward and backward scattering becoming lower.

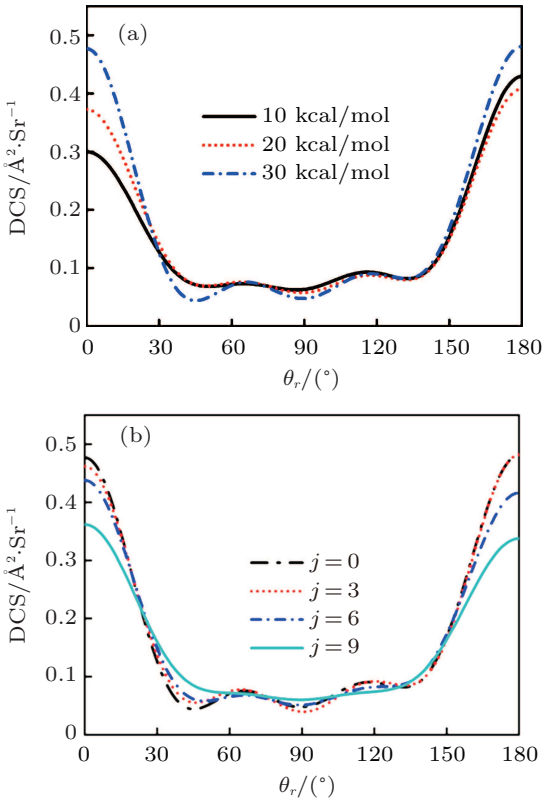



**Fig. 1.** (color online) The DCSs for the title H($^2$S) + NH ($a^1\Delta$) → $H_2(X^1\Sigma_g^+)$ + N ($^2$D) reaction at (a) collision energies of 10, 20, and 30 kcal/mol with $v = 0$, $j = 0$, and (b) at collision energy of 30 kcal/mol with $v = 0$, $j = 0$, 3, 6, 9, respectively.

To obtain a clearer understanding of the reaction mechanism, the variations of internuclear distances of $H_a$–$H_b$, $H_b$–N, and $H_a$–N are presented each as a function of propagation time based on these three collision energies in Fig. 2. The trajectories are selected in the scattering angle of 22.34°. Figures 2(a), 2(b), and 2(c), especially the first two, show that the attacking atom $H_a$ undergoes several collisions with the target molecule $H_b$–N and the complexes have relatively long lifetime before breaking up. The long-term survival of the metastable states could allow the system to perform extensive rotations before breaking up, thereby making the products come out in more random directions. So the indirect reactive trajectories, namely "trapped" trajectories, can be

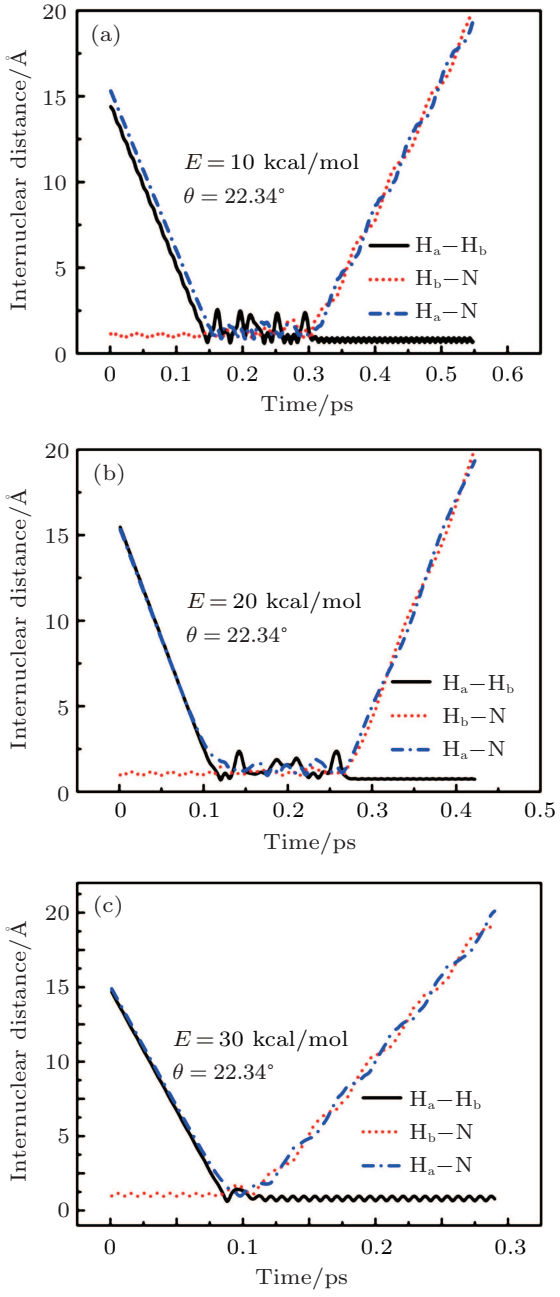



**Fig. 2.** (color online) Internuclear distances of $H_a$–$H_b$, $H_b$–N, and $H_a$–N each as a function of propagation time based on collision energies of (a) 10 kcal/mol, (b) 20 kcal/mol, and (c) 30 kcal/mol with scattering angle $\theta = 22.34°$.

observed. Therefore it is no surprise that the forward scattering and backward scattering are observed as can be seen in Fig. 1. The $H_a$–$H_b$ distance reaches its lowest value before the $H_a$–N does, that is to say, the attacking $H_a$ atom "hits" firstly on the $H_b$ atom of the target molecule and later migrates to form the $H_aN$ product. As a consequence, the reaction takes place by a migration mechanism.[45] Figure 3 shows the internuclear distances of $H_a$–$H_b$, $H_b$–N, and $H_a$–N each as a function of propagation time based on variation of initial reagent rotational excitations at 30 kcal/mol. It should be noted that the abstraction mechanism could be founded except for $j = 0$. That is to say, the initial reagent rotational excitation transforms the reaction mechanism from insertion to abstraction. And indirect reactive trajectories (i.e. many intermediate complexes appear) of interest are observed only when $j = 6$.

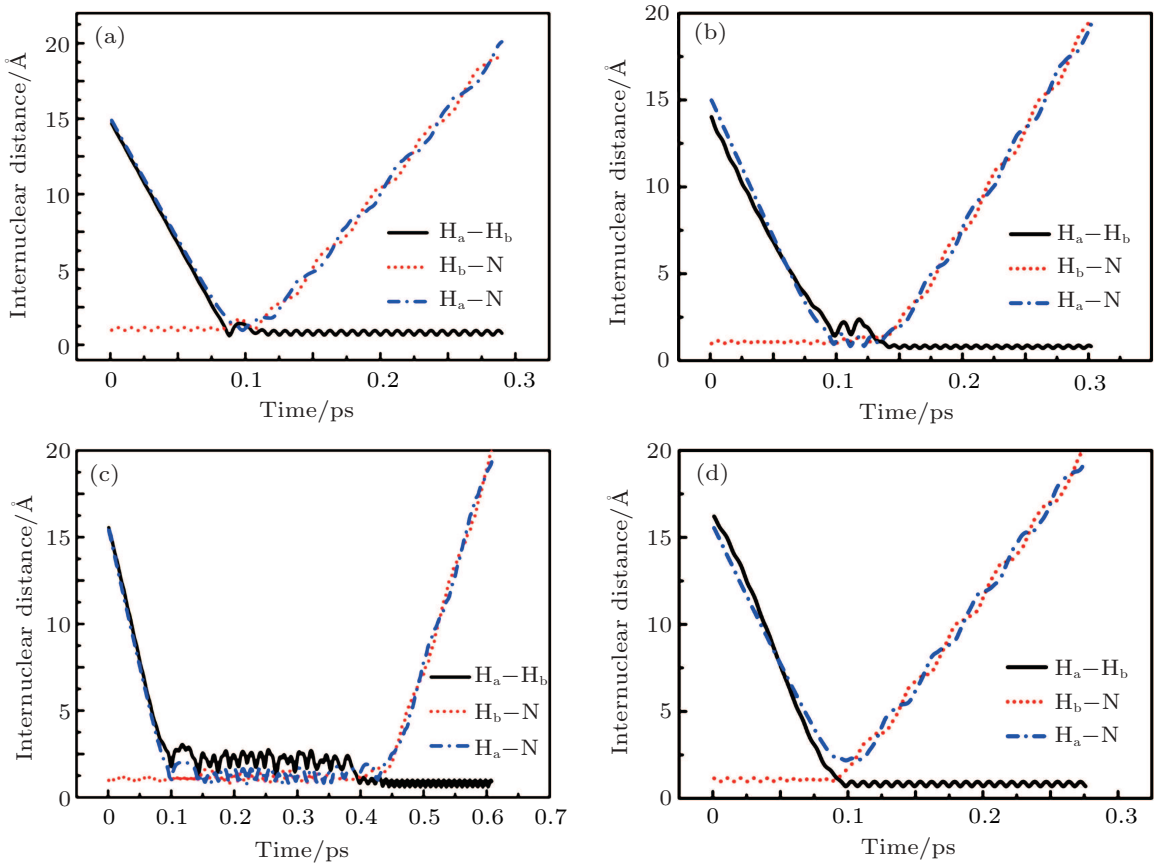



**Fig. 3.** (color online) Internuclear distances of $H_a$–$H_b$, $H_b$–N, and $H_a$–N each as a function of propagation time based on variations of initial reagent rotational excitations at 30 kcal/mol for the cases of $j = 0$ (a), 3 (b), 6 (c), and 9 (d).

### 3.2. Energy-dependent *k*–*j*′ and *k*–*k*′–*j*′ correlations

In this section, the energy-dependent behaviors of the angular distributions of $P(\theta_r)$ and $P(\phi_r)$ are discussed in detail, with the reactant NH selected at a specific initial state $v = 0$ and $j = 0$. The calculated distributions of $P(\theta_r)$ for the product $H_2$ molecule from $H(^2S)$ + NH $(a^1\Delta) \rightarrow H_2(X^1\Sigma_g^+)$ + N $(^2D)$ reaction under the collision energies 10 kcal/mol, 20 kcal/mol, and 30 kcal/mol are plotted in Fig. 4. Each of the distributions of $P(\theta_r)$, describing the $\boldsymbol{k}$–$\boldsymbol{j}'$ correlation, has a maximum at a $\theta_r$ angle value of 90° and symmetric with respect to 90°. It can be concluded that $\boldsymbol{j}'$ is distributed with cylindrical symmetry in the product scattering frame and the direction of $\boldsymbol{j}'$ is preferentially perpendicular to the k direction. As we can see, the distribution of $P(\theta_r)$ becomes weaker when the collision energy increases from 10 kcal/mol to 20 kcal/mol, while it becomes stronger when the collision energy increases from 20 kcal/mol to 30 kcal/mol. The product rotational alignment parameter $\langle P_2(\boldsymbol{j}'k)\rangle$ is used to investigate the trend of $P(\theta_r)$ distribution in depth, which are −0.3486, −0.3413, and −0.3683 at these three collision energies respectively (the closer to 0.5 the $\langle P_2(\boldsymbol{j}'k)\rangle$, the stronger the product alignment is). In the reaction process, the total angular momentum can be conserved as $\boldsymbol{L} + \boldsymbol{j} = \boldsymbol{j}' + \boldsymbol{L}'$, where $\boldsymbol{L}$ and $\boldsymbol{j}$ denote the orbital angular momentum and the rotational angular momentum respectively. When the rotational angular momentum of reactants is low (which is the case in H + NH ($v = 0$, $j = 0$)) $\boldsymbol{L} \approx \boldsymbol{j}' + \boldsymbol{L}'$. As the collision energy increases, the orbital angular momentum is also improved since the orbital angular momentum can be written as $L = b_{\max}(2\mu E_{\rm col})^{1/2}$ (although $b_{\max}$ decreases with collision energy, the degree of its reduction is incomparable to that of the collision energy increment). As a result, larger parts of $\boldsymbol{L}$ are disposed into $\boldsymbol{j}'$, which finally induces stronger alignment of $\boldsymbol{j}'$.

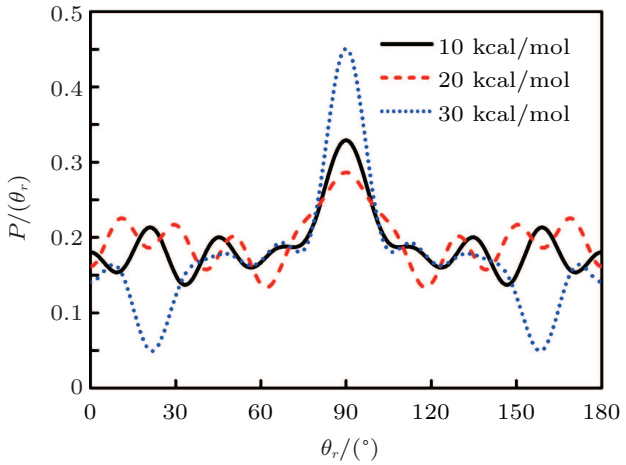



**Fig. 4.** (color online) Distributions of $P(\theta_r)$ for H($^2$S) + NH ($a^1\Delta$) ($v = 0$, $j = 0$) → $H_2(X^1\Sigma_g^+)$ + N ($^2$D) at collision energies of 10, 20, and 30 kcal/mol.

The dihedral angle distribution of $P(\phi_r)$ describing the $\boldsymbol{k}$–$\boldsymbol{k}'$–$\boldsymbol{j}'$ correlation is shown in Fig. 5, and it tends to be asymmetric with respect to the $\boldsymbol{k}$–$\boldsymbol{k}'$ scattering plane (or about $\phi_r = 180^\circ$) and could be used to reflect the strong polarization of product rotational angular momentum directly. In fact, the peaks in the distribution of $P(\phi_r)$ at $\phi_r$ angles close to 90° imply a preference for right-handed product rotation while the peaks at $\phi_r$ angles close to 270° indicate a preference for left-handed product rotation. The peaks of $P(\phi_r)$ appear at $\phi_r = 90^\circ$ and $\phi_r = 270^\circ$ indicate that the rotational angular momentum vectors of the products are mainly aligned along the $y$ axis of the CM frame. It can be seen that the peaks at $\phi_r = 90^\circ$ are stronger than those at $\phi_r = 270^\circ$ at these three collision energies, which means that the product rotational angular momentum vector $\boldsymbol{j}'$ is oriented along the positive direction of the $y$ axis. And the difference in peak between $\phi_r = 90^\circ$ and $\phi_r = 270^\circ$ increases with the increase of collision energy. It should be noted that the peaks of $P(\phi_r)$ distributions at higher collision energies are broader than those at lower collision energies which indicates that the rotation of the product molecule changes from the "in-plane" reaction mechanism into the "out-ofplane" mechanism. In turn, as depicted in Fig. 5, the $P(\phi_r)$ distributions each display a distinct 'V'-shaped splitting separately around $\phi_r = 90^\circ$ and 270° at 10 kcal/mol, which predicts a dynamic enhancement of the degree of orientation along the $y$ axis. A similar splitting was also found in the study of stereodynamics for reaction O + $H_2$.[46] The angular momentum polarization in the form of polar plot of the distribution of $P(\theta_r, \varphi_r)$ is also depicted in Fig. 6, which represents the scattering angle average of the full distribution of $P(\omega_t, \omega_r)$. The distributions of the $P(\theta_r, \phi_r)$ peaks at $(\pi/2, 3\pi/2)$ are in good accordance with the distributions of $P(\theta_r)$ and $P(\phi_r)$, which indicates that the HH products are preferentially polarized perpendicularly to the scattering plane.

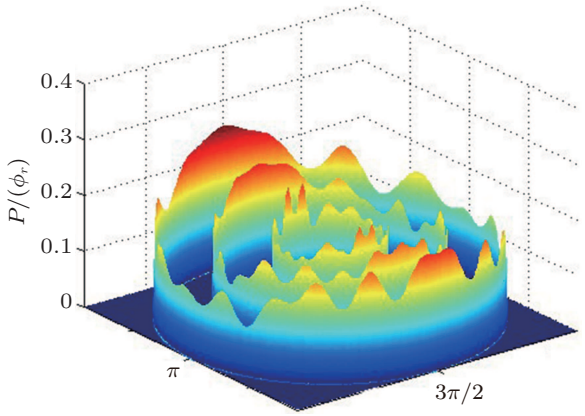



**Fig. 5.** (color online) Distributions of $P(\phi_r)$ for H($^2$S) + NH ($a^1\Delta$) ($v = 0$, $j = 0$) → $H_2(X^1\Sigma_g^+)$ + N ($^2$D) at three different collision energies of 10, 20, 30 kcal/mol from inner to outer.

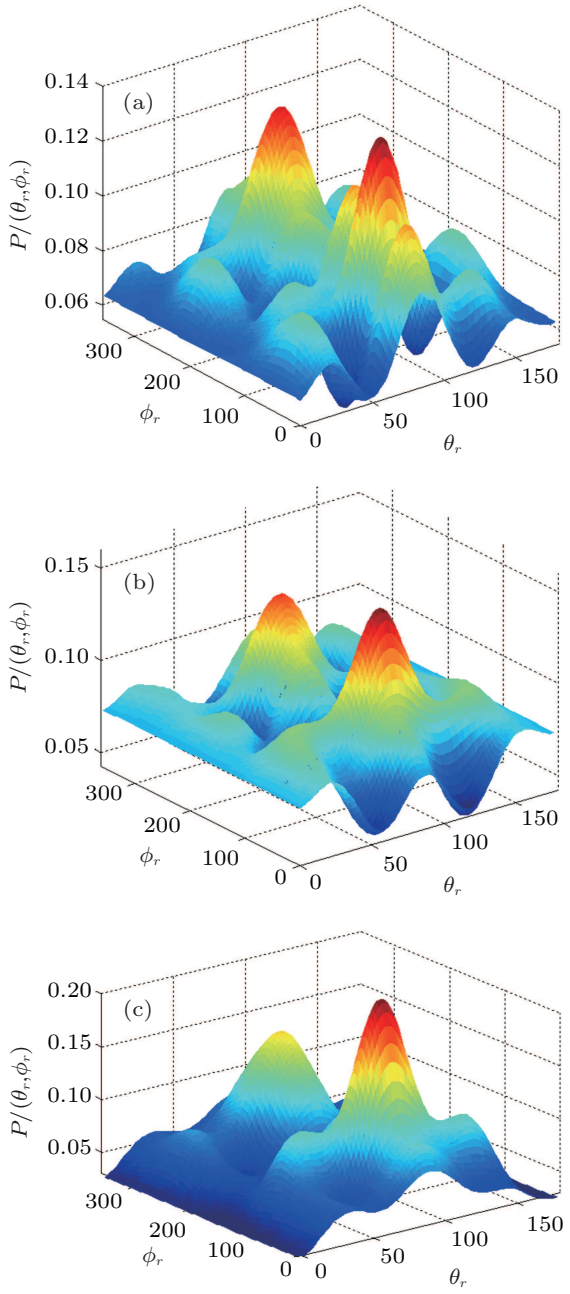



**Fig. 6.** (color online) $P(\theta_r, \phi_r)$ distributions averaged over all scattering angles at (a) 10 kcal/mol, (b) 20 kcal/mol, (c) 30 kcal/mol.

### 3.3. Rotation-dependent $k$–$j'$ and $k$–$k'$–$j'$ correlations

The effects of the initial rotational excitation of NH on the alignment of product angular momentum $\boldsymbol{j}'$ in the stereodynamics for the reaction H + NH ($v = 0$, $j = 0$, 3, 6, 9) are also investigated. The calculated results of $P(\theta_r)$ distribution for this reaction at 30 kcal/mol collision energy are shown in Fig. 7. It can be seen that the distributions of $P(\theta_r)$ become broader and lower when the reagent rotations are in the cases of $j = 3$, 6, 9, indicating that the product rotational alignment effect becomes weaker when the reagent is in the excited rotation state. This is also confirmed by the values of the product rotational alignment parameter $\langle P_2(\boldsymbol{j}'\boldsymbol{k})\rangle$, which are $-0.3683$, $-0.3460$, $-0.3546$, and $-0.350$ corresponding to $j = 0$, 3, 6, and 9, respectively. It should be emphasized that the few peaks of $P(\theta_r)$ distribution close to $\theta_r = 0°$ and 180° appear gradually with the enhancement of the initial rotational excitation of target molecular. It implies that as the initial rotational excitation of target molecular increases, the polarization parallel to the direction of the relative velocity of reactants appears, nothing but the degree of polarization is relatively weak.

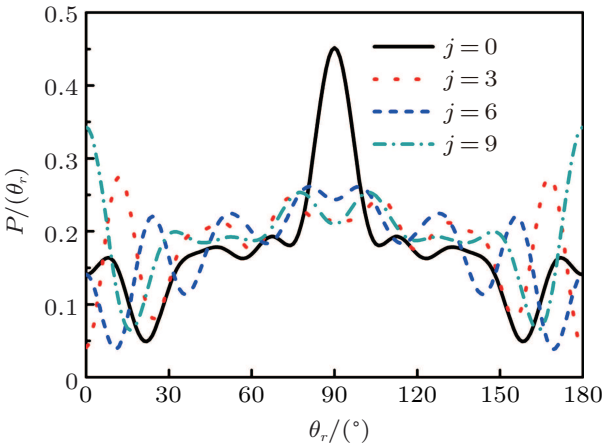



**Fig. 7.** (color online) Distributions of $P(\theta_r)$ for H($^2$S) + NH ($a^1\Delta$) ($v = 0$, $j = 0$, 3, 6, 9) → $H_2(X^1\Sigma_g^+)$ + N ($^2$D) at 30 kcal/mol.

In order to examine the influence of initial rotational state of NH on the orientation of product angular momentum $\boldsymbol{j}'$, we show the distributions of $P(\phi_r)$ in Fig. 8. The dihedral angle distribution of the $\boldsymbol{k}$–$\boldsymbol{k}'$–$\boldsymbol{j}'$ correlation shows that $P(\phi_r)$ tends to be asymmetric about $\phi_r = \pi$, reflecting the strong polarization of angular momentum directly. The product rotational angular momentum is not only aligned along the $y$ axis (i.e. the distributions have peaks at $\phi_r = \pi/2$ and $3\pi/2$ respectively), but is also oriented along the positive direction of the $y$ axis (i.e., the peaks at $\phi_r = \pi/2$ are larger than those at $\phi_r = 3\pi/2$). The $P(\phi_r)$ distribution peaking at $\phi_r$ angle close to $\pi/2$ implies a preference for right-handed HH rotation in planes that are parallel to the scattering plane. It is interesting to find that the reaction is symmetric around the relative velocity vector, while the distribution of $P(\phi_r)$ is asymmetric. The various angular distributions of the product reflect the vector correlation containing rich information about the angular momentum polarization. In order to validate the information about the product molecular axis polarization, the $P(\theta_r, \varphi_r)$ distributions averaged over all scattering angles for the reactions H($^2$S) + NH ($a^1\Delta$) ($v = 0$, $j = 0$, 3, 6, 9) → $H_2(X^1\Sigma_g^+)$ + N ($^2$D) are shown in Fig. 9. As can be seen, the distributions of $P(\theta_r, \phi_r)$ show peaks at $\theta_r = 90°$, $\phi_r = 90°$ and $\theta_r = 90°$, $\phi_r = 270°$, which are found to be in good accordance with the scenarios for the distributions of $P(\theta_r)$ and $P(\phi_r)$ of the HH products. The distributions of $P(\theta_r, \phi_r)$ indicate that the products of the reactions are mainly rotated in planes that are parallel to the scattering plane and the products are preferentially polarized perpendicularly to the scattering plane.

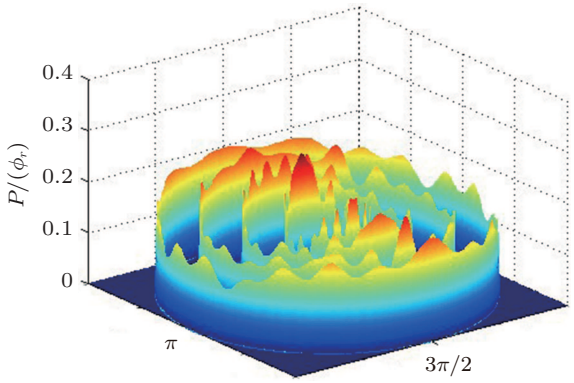



**Fig. 8.** (color online) Dihedral angle distributions of $P(\phi_r)$ for H($^2$S) + NH ($a^1\Delta$) → $H_2(X^1\Sigma_g^+)$ + N ($^2$D) from inner ($v = 0$, $j = 0$) to outer ($v = 0$, $j = 9$).

## 4. Conclusions

In the present work, the energy and rotation-dependent stereodynamics of the reaction H($^2$S) + NH ($a^1\Delta$) → $H_2(X^1\Sigma_g^+)$ + N ($^2$D) are studied based on the first excited state DMBE-SEC PES of $NH_2$ using QCT method. A total of $3 \times 10^4$ trajectories are run under each initial condition to investigate the effects of collision energy and rotational state of NH radical on the product rotational polarization. With the increase of the collision energy, both forward and backward scatterings become stronger, in which the forward scattering has a bigger magnitude of variation. The influence of collision energy on the $\boldsymbol{k}$–$\boldsymbol{k}'$ distribution can be attributed to a purely impulsive effect, and also used to control the reaction mechanism. Whereas with the increase of rotational quantum number, both forward scattering and backward scatterings become lower. It can be explained as the fact that the rotational excitation enlarges the rotational rate of reagent NH in the entrance channel to reduce the probability of collision between incidence H atom and H atom of target molecule. In addition, initial reagent rotational excitation can convert the insertion mechanism into the abstraction mechanism under the condition of high collision energy.

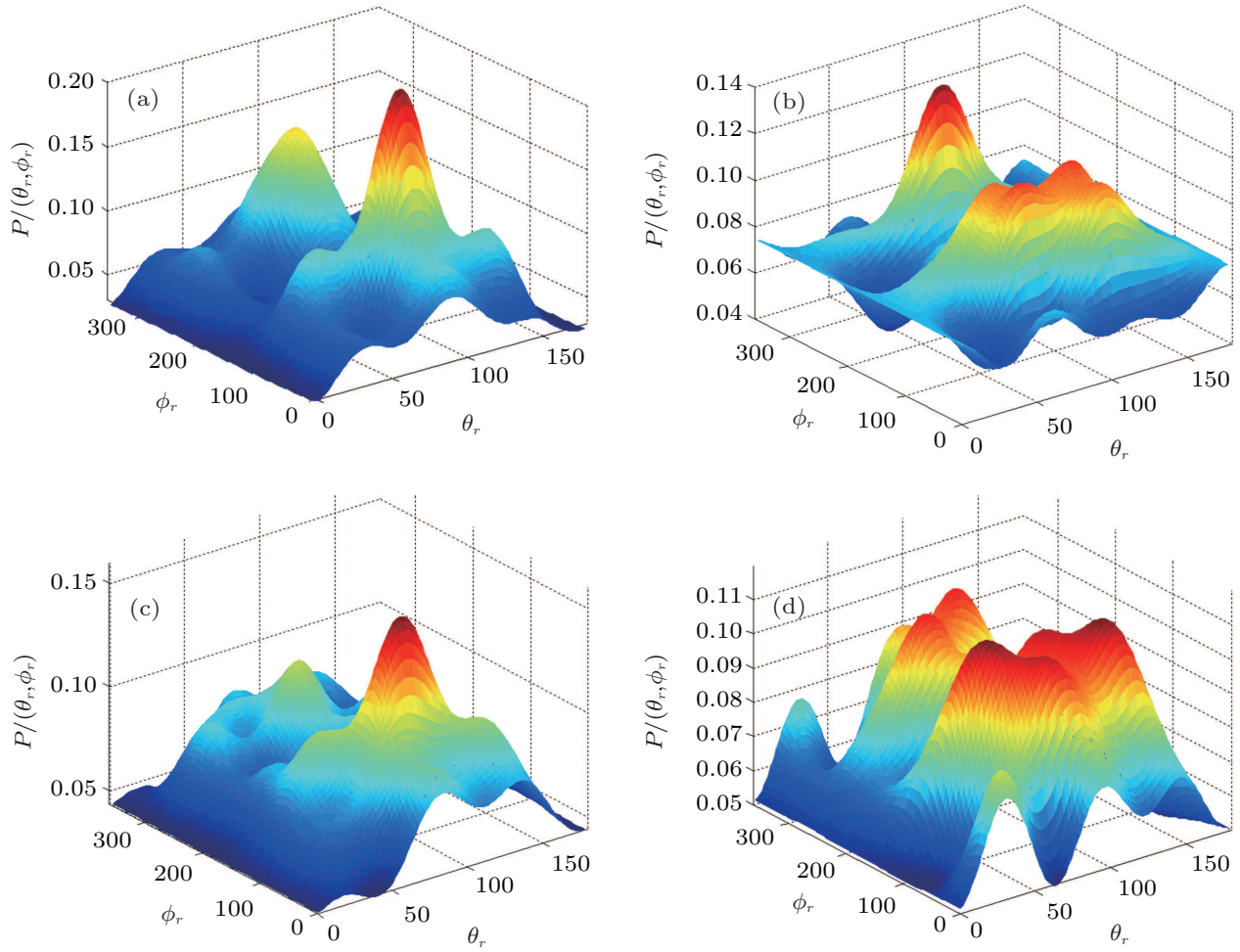



**Fig. 9.** (color online) $P(\theta_r, \phi_r)$ distributions for the reactions $H(^2S) + NH(a^1\Delta)$ ($v = 0$, $j = 0, 3, 6, 9$) $\rightarrow H_2(X^1\Sigma_g^+) + N(^2D)$ (from (a) to (d)) at the collision energy of 30 kcal/mol.

The results of vector correlation show that the product rotational angular momentum $\boldsymbol{j}'$ is not only aligned, but also oriented along the direction perpendicular to the scattering plane. It is found that the three angle distributions are sensitive to initially collision energy and rotational excitation.

## References


[1] Wright C A and Winkler A N 1968 *Active Nitrogen* (New York: Academic)

[2] Alagia M, Balucani N, Cartechini L, Cachavecchia P, Volpi G G, Pederson L A, Schatz G C, Lendvay G, Harding L B, Hollebeek T, Ho T S and Rabitz H 1999 *J. Chem. Phys.* **110** 8857

[3] Dodd J A Lipson S J Flanagan D J, Blumberg W A M Pearson J C and Green B D 1991 *J. Chem. Phys.* **94** 4301

[4] Umemoto H and Matsumoto K 1996 *J. Chem. Phys.* **104** 9640

[5] Umemoto H, Asai T and Kimura Y 1997 *J. Chem. Phys.* **106** 4985

[6] Li Y Q and Varandas A J C 2010 *J. Phys. Chem. A* **114** 9644

[7] Li Y Q, Song Y Z, Song P, Li Y Z, Ding Y, Sun M T and Ma F C 2012 *J. Chem. Phys.* **136** 194705

[8] Funken K, Engels B, Peyerimhoff S D and Grein F 1990 *Chem. Phys. Lett.* **172** 180

[9] Chu T S and Han K L 2005 *J. Phys. Chem. A* **109** 2050

[10] Chu T S, Han K L and Varandas A J C 2006 *J. Phys. Chem. A* **110** 1666

[11] Chu T S, Zhang Y and Han K L 2006 *Int. Rev. Phys. Chem.* **25** 201

[12] Chu T S and Han K L 2008 *Phys. Chem. Chem. Phys.* **10** 2431

[13] Chu T S, Lu R F, Han K L, Tang X N, Xu H F and Ng C Y 2005 *J. Chem. Phys.* **122** 244322

[14] Brandi R, Leonardi E and Petrongolo C 1997 *J. Phys. Chem. A* **101** 5696

[15] Peyerimhoff S D and Buenker R J 1979 *Can. J. Chem.* **57** 3182

[16] Takayanagui T, Kobayashi H and Tsunashima S 1996 *J. Chem. Soc. Faraday Trans.* **92** 1311

[17] Li Y Q and Varandas A J C 2010 *J. Phys. Chem. A* **114** 6669

[18] Pederson L, Schatz G, Hollebeek T, Ho T S, Rabitz H and Harding L B 2000 *J. Phys. Chem. A* **104** 2301

[19] Jensen P Buenker R J Hirsch G and Rai S N 1990 *Mol. Phys.* **70** 443

[20] Li Y Q, Ma F C and Sun M T 2013 *J. Chem. Phys.* **139** 154305

[21] Rodrigues S P J, Fontes A C G, Li Y Q and Varandas A J C 2011 *Chem. Phys. Lett.* **516** 17

[22] Suzuki T, Shihira Y, Sato T, Umemoto H and Tsunashima S 1993 *J. Chem. Soc. Faraday Trans.* **89** 995

[23] Buenker R J, Peric M Peyerimhoff S D and Marian R 1981 *Mol. Phys.* **43** 987

[24] Li Y Q Yuan J C, Chen M D, Ma F C and Sun M T 2013 *J. Comput. Chem.* **34** 1686

[25] Pederson L A, Schatz G C, Ho T, Hollebeek T, Rabitz H and Harding L B 1999 *J. Chem. Phys.* **110** 9091

[26] Qu Z, Zhu H, Schinke R, Adam L and Hack W 2005 *J. Chem. Phys.* **122** 20431

[27] Vetter R, Zülicke L, Koch A, Van D E F and Peyerimhoff S D 1996 *J. Chem. Phys.* **104** 5558

[28] Zhou S L, Xie D, Lin S Y and Guo H 2008 *J. Chem. Phys.* **128** 224316

[29] Varandas A J C and Poveda L A 2006 *Theor. Chem. Acc.* **116** 404

[30] Bella S and Schaefer H F 1977 *J. Chem. Phys.* **67** 5173

[31] Li X Wang M Pino I Yang C and Ma L 2009 *Phys. Chem. Chem. Phys.* **11** 10438

[32] Li X Wang M Pino I Yang C and Wu J 2010 *Phys. Chem. Chem. Phys.* **12** 7942
[33] Adam L, Hack W, McBane G C, Zhu H and Schinke W R 2007 *J. Chem. Phys.* **126** 034304
[34] Wang M L Han K L and He G Z 1998 *J. Phys. Chem. A* **102** 20204
[35] Wang M L Han K L and He G Z 1998 *J. Chem. Phys.* **109** 5446
[36] Chen M D Han K L and Lou N Q 2002 *Chem. Phys.* **283** 463
[37] Chen M D Han K L and Lou N Q 2003 *J. Chem. Phys.* **118** 4463
[38] Zhang X and Han K L 2006 *Int. J. Quanttum Chem.* **106** 1815
[39] Han K L, He G Z and Lou N Q 1996 *J. Chem. Phys.* **105** 8699
[40] Cheng D H, Yuan J C and Chen M D, 2014 *J. Phys. Chem. A* **1** 55
[41] Liu S L and Shi Y 2010 *Chin. Phys. Lett.* **27** 123103
[42] Ding Y J and Shi Y 2011 *Comput. Theor. Chem.* **963** 306
[43] Zhang Y Y, Shi Y, Xie T X, Jin M M and Hu Z 2013 *Chin. Phys. B* **22** 083402
[44] Gray S K, Goldfield E M, Schatz G C and Balint-Kurti G G 1999 *Phys. Chem. Chem. Phys.* **1** 1141
[45] Duan Z X, Li W L and Qiu M H 2012 *J. Chem. Phys.* **136** 144309
[46] Alexander A J Aoiz F J Banares L Brouard M and Simons J P 2000 *Phys. Chem. Chem. Phys.* **2** 571